Journal of Nuclear Materials 117 (1983) 55–63
North-Holland Publishing Company

PRECIPITATE DISSOLUTION BY HIGH ENERGY COLLISION CASCADES *

Philip CHOU and N.M. GHONIEM

Fusion Engineering and Physics Group, School of Engineering and Applied Science, University of California at Los Angeles, Los Angeles, CA 90024, USA

The evolution of the microstructure during irradiation is now widely recognized due to: (1) radiation altered kinetic phenomena; (2) collisional processes by energetic cascades. In this paper, we investigate the specific nature of the collisional interaction between energetic cascades and precipitates. A new Monte Carlo-based computer program, TRIPOS, has been developed for the TRansport of Ions in POlyatomic Solids. The computer code utilizes standard nuclear and electronic energy loss formulas, and compares well with experimental data on particle reflection, penetration and sputtering. One of the unique features of the code is its applicability to problems involving multispecie media in multilayers of 3-dimensional configurations. The interaction of neutron-initiated high energy collision cascades is demonstrated to result in the partial dissolution of precipitates. However, the maximum precipitate size that may be completely destroyed by a high energy collision cascade is only a small fraction of the cascade size. Matrix atom implantation inside precipitates as well as preferential sputtering of light atoms from the surface of precipitates into the matrix is demonstrated to lead to changes in precipitate stoichiometry.

1. Introduction

The instability of structural alloys under irradiation is of primary concern to nuclear industry technologists, since slight changes in such stability can be reflected in dramatic modifications to material properties. Many examples exist in the literature where irradiation results in an alteration of known thermodynamic equilibrium conditions. Experimental observations include dissolution of precipitates, re-solution of gas atoms in bubbles, disordering and re-ordering effects, and the formation of new or "wrong" phases. Several reviews of the subject exist [1–7], where the instability of irradiated alloys is extensively discussed.

Microstructural modifications by irradiation are now recognized to result from two broad categories: (1) radiation altered kinetic phenomena; and (2) collisional processes by energetic cascades. The first category involves diffusional mechanisms that are strongly influenced by the presence of radiation produced defects, while the second category is a result of dynamic energy exchanges between the PKA and the matrix atoms.

The propagation of energetic cascades can result in both the dissolution of precipitates and the disordering of ordered structures. In an irradiation environment, a balance may be achieved between dissolution or disordering on one hand and radiation enhanced diffusion on the other. One of the mechanisms is usually more dominant, depending on the temperature and irradiation conditions. At low temperature and for high displacement damage rates, the dissolution of precipitates is more dominant than their re-formation. The present work is a theoretical study of the detailed energetics of cascade effects on precipitates. As such, we will not attempt to model the re-formation process by atomic diffusion. It has been pointed out [4] that experiments have illustrated precipitate dissolution, providing evidence that whole precipitates, smaller than a collision cascade, can be dissolved in a single event [7].

Nelson et al. [3] proposed two mechanisms for the radiation enhanced dissolution of precipitates. The first process was viewed as an internal sputtering mechanism, where dynamic collision events which occur as a result of displacement cascades cause atoms within the precipitate to recoil into the surrounding matrix. On the other hand, a disordering effect was proposed, in which cascades essentially destroy the ordered precipitate structure. Diffusion was assumed to order the innermost parts of the precipitate while atoms on the periphery are lost to the matrix. No detailed model has been presented in the open literature to quantify these assumptions, and it is likely that a combination of these mechanisms control the process.

Calculations of displacement damage in precipitates

* Work is partially supported by the National Science Foundation, Grant # CPE81-15771 with UCLA.

0022-3115/83/0000–0000/$03.00

is complicated by many factors:

(1) The geometry of a precipitate particle is not amenable to simple mathematical descriptions;
(2) The damage is produced in both the matrix and the precipitate, i.e., a multi-layer, polyatomic medium; and
(3) Precipitate–matrix interface properties are not very well characterized.

Damage calculations in a polyatomic medium have been performed by Winterbon [8] for the diatomic systems UC and UO_2. A number of investigators have also attempted to calculate the damage energy in polyatomic solids. Recently, Coulter and Parkin [9] integrated the polyatomic Lindhard equations for each atom type in a number of diatomic and triatomic materials. They concluded that the effect of combining different atom types in a polyatomic material is to reduce the damage efficiency relative to an average monatomic material.

The present study is a Monte Carlo numerical simulation of the displacement damage process in a multilayer, polyatomic medium. This avoids placing unrealistic approximations to the solution of Lindhard-type equations using analytical or direct numerical methods.

In the following section, we present the theoretical basis for the solution of the problem. This is followed by the Monte Carlo Code description and verification. We then describe and define the particular problem of precipitate dissolution. The results and conclusions are finally presented.

2. Theoretical analysis

Computer simulations of ion transport in solids using the Monte Carlo method have been previously reported [10–14]. The major differences between these computer codes are summarized in their choice of a crystalline or amorphous solid, and in their treatment of the elastic (nuclear) scattering. Recently, Biersack and Haggmark [13] developed a successful code for the transport of energetic ions in amorphous targets (TRIM). In their analysis, the Moliere approximation [15] to the Thomas–Fermi potential was used in an approximate analytical formulation of the scattering angle at low energy. At high energy, the unscreened coulomb potential was found to be sufficient. The program was designed to provide information on ion range and damage characteristics as well as reflection and transmission properties of planar targets. Another version of this code, MORELOVE, is being developed for multi-layer targets with polyatomic compositions. For applications in which the crystalline nature of the solid is important, Oen and Robinson [10] developed the widely used MARLOWE computer program.

Our work, which is based upon the Monte Carlo solution to the transport equation in an amorphous solid, is a new contribution to this area. The computer code developed in this work is primarily for the TRansport of Ions in POlyatomic Solids, and will be referred to as TRIPOS for convenience. The theoretical methods contained in the code differ from other treatments [10–14], and in particular from the TRIM program. A summary of some of the basic differences between TRIM and the present work (TRIPOS) is given in table 1.

2.1. Scattering cross-section

The power law approximation to the Thomas–Fermi potential is used in our analysis. Simple analytical expressions are available for any assumed power (s) for the radial dependence of the interaction potential. At high energies, the power (s) is set $s = 1$, and the interaction between two atoms is purely coulombic. For lower incident particle energies, higher degrees of screening occur for the pure coulomb field and the power index, s, can be different from unity. At still lower energies, the interatomic potential can be best represented by a Born–Mayer potential.

In this case, the differential cross-section for the power law potential is given by

$$d\sigma(E, T) = C_m E^{-m} T^{-1-m} dT, \tag{1}$$

$$\text{where } C_m = \frac{\pi}{2} \lambda_m a_{12}^2 \frac{M_1}{M_2} \left(\frac{2 Z_1 Z_2 e^2}{a_{12}} \right)^{2m} \tag{2}$$

Table 1
Comparison between TRIM and TRIPOS

	TRIM	TRIPOS
Purpose:	– for ion–solid interactions in single specie media	– for ion–solid interactions in polyatomic media
Method used	– Moliére potential	– continuous power law potentials
	– neglect small angle nuclear scattering	– consider small angle nuclear scattering
	– constant collision distance	– free path collision distance is selected from a probability distribution
Agreement and computing speed	comparable	

and

M_1, Z_1 = mass and charge of incident particle,
M_2, Z_2 = mass and charge of recoil particle,
E = incident particle energy,
T = recoil energy.

$$a_{12} = 0.4683 \left(Z_1^{2/3} + Z_2^{2/3} \right)^{-1/2} \text{ Å}, \tag{3}$$

$$m = 1/s, \tag{4}$$

$$\left.\begin{aligned} (m, \lambda_m) &= \left(\tfrac{1}{3}, 1.309\right) && \text{for } E_A \le E \le E_B \\ &= \left(\tfrac{1}{2}, 0.327\right) && \text{for } E_B \le E \le E_C \\ &= (1, 0.5) && \text{for } E_c \le E \end{aligned}\right\}. \tag{5}$$

The values of m and λ_m are taken from ref. 16. For lower energies ($E \lesssim E_A$), the differential cross-section for Born–Mayer interaction is represented with a power approximation of $(m, \lambda_m) = (0, 24)$, and $a_{12} = 0.219$ Å [17].

A major problem with the use of the power law approximation is the determination of the transition energies E_A, E_B and E_c; such that the results are accurate. Based upon range considerations, Winterbon [16] determined these transition energies. In the present work, we determine transition energies by requiring the continuity of the *total* nuclear stopping power, $S_n(E)$. The quantity $S_n(E)$ is therefore continuous across an energy boundary.

$$S_n(E) = \int_{T_s}^{\Lambda E} T \mathrm{d}\sigma(E, T), \tag{6}$$

$$= \frac{C_m}{1-m} \Lambda^{1-m} E^{1-2m}, \quad m \neq 1, \tag{7}$$

$$= \frac{C_1}{E} \ln\left(\frac{\Lambda E}{T_s} \right), \quad m = 1, \tag{8}$$

where

$$\Lambda = 4M_1M_2/(M_1 + M_2)^2. \tag{9}$$

Λ is the maximum fractional energy transferred in a collision, and T_s is the smallest value (cut off) of transferrred energy. A set of continuity equations is solved resulting in the unique determination of E_A, E_B, and E_c. The value of T_s as function of E is the energy transferred for an impact parameter equal to one half the interatomic spacing.

2.2. Free path between collisions

The total nuclear scattering cross-section for charged particle interaction in a binary collision can be expressed in the form:

$$\sigma(E) = \frac{C_m}{m} E^{-m} \left[T_s^{-m} - (\Lambda E)^{-m} \right], \quad m \neq 0, \tag{10}$$

$$= C_0 \ln(\Lambda E / T_s), \quad m = 0, \tag{11}$$

where C_m is the constant used in the power law approximation [eq. (2)]. In our treatment of energy loss, energy transfers below T_s are treated in a continuous way and added to the electronic energy loss, as will be shown later.

The probability of a particle undergoing a binary collision after moving a distance Δl in the solid is given by

$$P = 1 - \exp[-N\sigma(E)\Delta l], \tag{12}$$

where N is the atomic density of the solid. This assumes a decoupling of electronic and nuclear energy losses. A random number, R_1, is generated for an even distribution of P between 0 and 1. The distance between collisions is therefore determined by

$$\Delta l = \frac{1}{N\sigma(E)} \ln\left(\frac{1}{1 - R_1'} \right) = \frac{1}{N\sigma(E)} \ln\left(\frac{1}{R_1} \right), \tag{13}$$

where R_1 and R_1' have the same probability distribution.

2.3. Type of recoil

In the binary collision approximation, a moving atom can interact with only one medium atom at a time. If the moving atom is in a polyatomic medium, it is necessary to determine the interaction probabilities with each of the components of the polyatomic medium. To implement this, we first calculate the total cross section for the interaction, $\Sigma_T(E)$, which is defined as

$$\Sigma_T(E) = \sum_{i=1}^{NM} \Sigma_i(E), \tag{14}$$

where NM is the total number of species in the polyatomic medium. $\Sigma_i(E)$ is the total cross-section for species i at energy E. We also define a partial total cross-section $\Sigma_{TP}(E)$ as follows:

$$\Sigma_{TP}(E) = \sum_{i=1}^{NP} \Sigma_i(E), \qquad 1 \le NP \le NM. \tag{15}$$

The commulative distribution function is therefore $\xi_{NP} = \Sigma_{TP}(E)/\Sigma_T(E)$, which is bounded between 0 and 1. A random number, R_2, is then generated; and if $\xi_{NP-1} < R_2 \le \xi_{NP}$, a type NP atom is chosen for the collision of interest.

2.4. Scattering angle

The scattering angle in a collision is determined here from cross section information, whereas in TRIM [13] it is calculated by assuming a distribution of impact parameters. Transferred energy to the recoil is simply proportional to the differential cross-section. From the cumulative distribution function (cdf), a random number, R_3, is related to the transferred energy, T, and the incident energy, E, by

$$\left.\begin{aligned} R_3 &= \frac{T_s^{-m} - T^{-m}}{T_s^{-m} - (\Lambda E)^{-m}}, && m \neq 0, \\ &= \frac{\ln(T/T_s)}{\ln(\Lambda E/T_s)}, && m = 0. \end{aligned}\right\} \tag{16}$$

Eq. (16) is easily solved for the transferred energy, which leads to

$$\left.\begin{aligned} T &= \left[T_s^{-m}(1-R_3) + R_3(\Lambda E)^{-m}\right]^{-1/m}, && m \neq 0, \\ &= (\Lambda E)^{R_2} T_s (1-R_3), && m = 0. \end{aligned}\right\} \tag{17}$$

The determination of the scattering angle, θ, in the center of mass system (CMS) is achieved by using the well known kinematic relation

$$\theta = 2\sin^{-1}(T/\Lambda E)^{1/2}. \tag{18}$$

In the laboratory system, the scattering angle, ψ, is given by

$$\psi = \tan^{-1}\left(\frac{\sin\theta}{\cos\theta + (M_1/M_2)}\right). \tag{19}$$

The azimuthal scattering angle is finally selected using the relation

$$\phi = 2\pi R_4, \tag{20}$$

where R_4 is a random number uniformly distributed between 0 and 1.

The angles for recoils are given by

$$\psi_R = \tan^{-1}[\sin\theta/(1-\cos\theta)], \tag{21}$$

$$\phi_R = 2\pi R_4 - \pi. \tag{22}$$

2.5. Particle position

The scattering angles described in the previous section are determined with reference to the incident particle direction. In a fixed frame of reference, however, the direction cosines of the particle velocity vector must be calculated after each collision. Let $(\alpha_i, \beta_i, \gamma_i)$ be the direction cosines of the particle after the ith collision. It can be easily shown that

$$\alpha_i = \alpha_{i-1}\cos\psi + \sin\psi(\gamma_{i-1}\alpha_{i-1}\cos\phi - \beta_{i-1}\sin\phi)/\left(1-\gamma_{i-1}^2\right)^{1/2}, \tag{23}$$

$$\beta_i = \beta_{i-1}\cos\psi + \sin\psi(\gamma_{i-1}\beta_{i-1}\cos\phi + \alpha_{i-1}\sin\phi)/\left(1-\gamma_{i-1}^2\right)^{1/2}, \tag{24}$$

$$\gamma_i = \gamma_{i-1}\cos\psi + \left(1-\gamma_{i-1}^2\right)^{1/2}\sin\psi\cos\phi. \tag{25}$$

The position of the particle at the point of collision, i, is given by

$$X_i = X_{i-1} + \alpha_{i-1}\Delta l, \tag{26}$$

$$Y_i = Y_{i-1} + \beta_{i-1}\Delta l, \tag{27}$$

$$Z_i = Z_{i-1} + \gamma_{i-1}\Delta l. \tag{28}$$

The position of the particle is checked in relationship to the surface boundary. This information is used for the determination of sputtering events and particle history termination.

2.6. Electronic and small angle nuclear energy losses

The energy transferred between electrons and a moving atom is very small and much more frequent than atom–atom collisions. Also, for large impact parameters the nuclear scattering energy loss is small and has been neglected in many previous treatments [11,13]. It is possible, therefore, to treat both the electronic and low angle nuclear scattering energy losses in a continuous way. We will first describe the treatment of electronic energy loss, and then show how we include nuclear collisions that result in an energy transfer below T_s.

For ion velocities $v < v_0 Z_1^{2/3}$, where $v_0 = e^2/h \simeq c/137$ and c is the speed of light, the electronic stopping is represented by the Lindhard–Scharff formula.

$$[S_e(E)]_{LS} = \frac{1.212 Z_1^{7/6} Z_2}{\left(Z_1^{2/3} + Z_2^{2/3}\right)^{3/2} M_1^{1/2}} E^{1/2} \text{ eV Å}^2. \tag{29}$$

At higher particle velocities, $v > v_0 Z_1^{2/3}$, the Bethe–Bloch formula is used. It has the form

$$[S_e(E)]_{BB} = \frac{8\pi Z_1^2 e^4}{I_0 \epsilon_B} \ln(\epsilon_B) \tag{30}$$

and

$$\epsilon_B = 4\frac{m_e}{M_1}\frac{E}{Z_2 I_0}, \tag{31}$$

where $(Z_2 I_0)$ is the mean excitation energy. I_0 is the

Bloch constant given by

$$\left.\begin{aligned} I_0 &= 12 + 7Z_2^{-1}\ \text{eV}, && Z_2 < 13, \\ &= 9.76 + 58.5Z_2^{-1.19}\ \text{eV}, && Z_2 \geq 13. \end{aligned}\right\} \quad (32)$$

In the intermediate regime, there is no simple analytical formula for S_e. In order to bridge this gap, where $v \sim v_0 Z_1^{2/3}$, an interpolation scheme proposed by Biersack [13] is used.

$$[S_e]^{-1} = [S_e]_{LS}^{-1} + [S_e]_{BB}^{-1}. \quad (33)$$

Now we turn our attention to small angle nuclear energy loss. In order to render the total nuclear scattering cross-section finite, the lower limit on energy transfers is set to a small value, T_s. This value corresponds to an impact parameter of half the interatomic spacing. Below T_s, small amounts of energy are transferred in collisions, yet they contribute to total energy loss because of the high probability of their occurrence. It is necessary to keep good energy accounting in this energy range. The following quantity is therefore evaluated and added to the electronic energy loss.

$$\left.\begin{aligned} S_{ns}(E) &= \int_{T_c}^{T_s} T\,d\sigma, \\ &= \frac{C_m}{(1-m)} \Lambda^{1-m} E^{-m} \left(T_s^{1-m} - T_c^{1-m}\right), && m \neq 1, \\ &= \frac{C_1}{E} \ln\left(\frac{T_s}{T_c}\right), && m = 1, \end{aligned}\right\} \quad (34)$$

where T_c is of the order of a few eV's.
The total "continuous" energy loss is therefore

$$\Delta E_{en} = [S_e(E) + S_{ns}(E)] N \Delta l. \quad (35)$$

2.7. Particle history termination and sputtering

A particle history is terminated in two cases: (1) if its energy falls below a minimum value, which is the displacement threshold energy (E_d) in the bulk or the surface binding energy (E_{SB}) near the surface; and (2) if it physically leaves the boundary of interest with low energy.

Calculations of sputtering into vacuum are sensitive to the surface binding energy. In our work the plannar potential barrier to the surface binding energy is used for slab geometry. The binding energy, U, at an ejection direction cosine with plane normal, μ, is given by

$$U(\mu) = U_0/\mu^2, \quad (36)$$

where U_0 is the minimum energy for particle history termination. For spherical geometry

$$U(\mu) = U_0. \quad (37)$$

Internal sputtering of atoms is treated in a different way. The minimum energy for an atom at the precipitate–matrix interface to be ejected is taken as its bulk displacement energy in a single specie medium.

3. Verification of TRIPOS

The major motivation behind the development of this work is to construct a computer code for general use in real alloys with multilayers of polyatomic material. The program has options to analyze surface physics problems, such as reflection, sputtering, range, and deposited damage. Also, it contains capabilities for bulk radiation damage problems, such as re-solution of gas atoms from bubbles, dissolution of precipitate particles, defect generation, and modifications of general microstructure by energetic cascades. Problems with slab or spherical geometries are handled by the present version of the code.

Fig. 1 shows a comparison between the results of TRIPOS and the crystalline Monte Carlo Code MARLOWE for the reflection coefficient of $^4_2$He on copper. The standard deviation is shown on the particle reflection coefficient for 1000 histories. The range results of the same problem are compared to TRIM in fig. 2. The same figure also shows the comparison for 1 keV

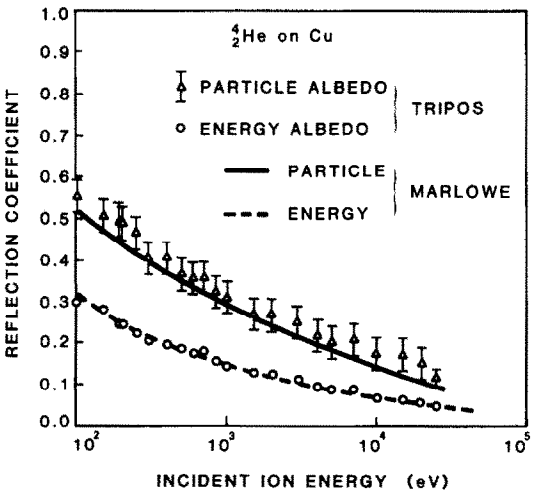

Fig. 1. Comparison between TRIPOS and MARLOWE for particle and energy reflection coefficients of $^4_2$He on Cu at normal incidence.

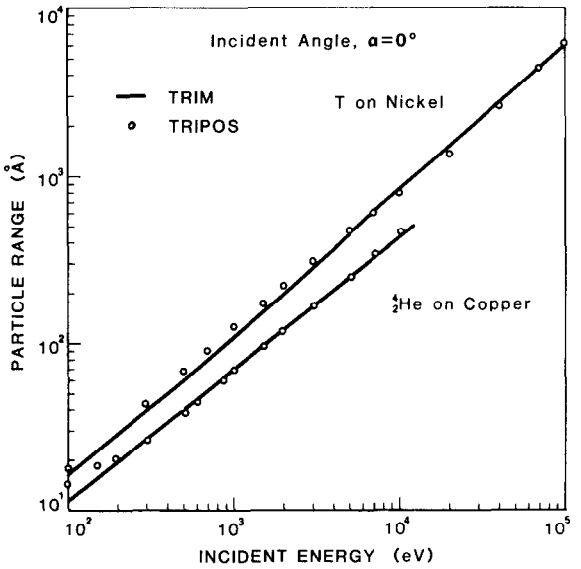

Fig. 2. Comparison between TRIM and TRIPOS for the range of T on Ni and $^4_2$He on Cu at normal incidence as a function of energy.

tritium on nickel at normal incidence. In order to proceed with calculations of precipitate dissolution, the capabilities of the code to deal with sputtering problems have to be tested. Fig. 3 shows the sputtering coefficient defined as the ratio of sputtered to incident atom ratio as a function of incident angle for 4 keV alpha particles on nickel [18]. The figure is a comparison between TRIPOS, TRIM, and experimental data by Bay and Bohdansky [19]. It is to be noted that the angle for

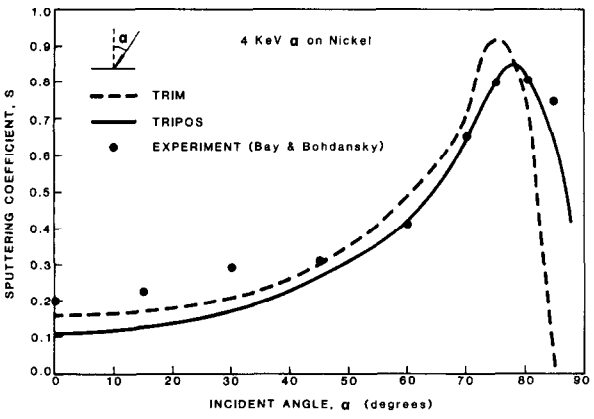

Fig. 3. Comparison between TRIPOS, TRIM and experiment for the sputtering coefficient of 4 keV $^4_2$He on Ni as a function of incident angle.

maximum sputtering coefficient as calculated by TRIPOS is coincident with the experimental data.

4. Results

The problem of precipitate dissolution in complex alloys has been given only a simplified analysis in the past [4]. Recognizing the importance of phase stability in structural materials, more detailed experiments and theoretical analyses are felt to be necessary. In the present study, we have made the following reasonable assumptions:

(1) The irradiation temperature is low. Therefore, diffusion of atoms sputtered away from the precipitate is not considered.
(2) Precipitates are assumed to have the same average size, and are distributed homogeneously in the matrix.
(3) Other microstructural features (voids, dislocations, etc.) are not modeled in the study.
(4) Instantaneous cascade restructuring is not considered.

A cell approach is used to study the interaction of collision cascades with precipiate particles. The cell is composed of two concentric spheres, the inner being the precipitate particle and the outer is determined by the density of precipitates. Since precipitates occupy only a small fraction of the matrix volume, most of the high energy collision cascades will propagate through the matrix rather than the precipitate structure.

To be specific, we will concentrate here on the study of MC-type precipitates in steels. The stoichiometric composition is taken as $M_{23}C_6$. To determine the nature of the interaction between a precipitate and a high energy collision cascade, it is important to study the effects of the cascade size and position in relation to the precipitate size. Generally speaking, two types of interactions may occur between cascades and precipitates. First, direct dissolution of precipitate atoms takes place if cascades are initiated within the precipitate boundary. And second, cascades initiated in the matrix with a chance to arrive at the precipitate will lead to indirect dissolution.

It is important to determine, for a given neutron energy spectrum, the maximum precipitate size which can be completely destroyed in an interaction with a single collision cascade. To study this aspect, we define the dissolution efficiency, η_{Dis}, as the fraction of precipitate atoms sputtered into the matrix by a single collision cascade. It is also possible that a collision cascade results in implantation of matrix atoms into the

precipitate, thereby altering its composition. We therefore define the implantation efficiency, η_{Imp}, as the ratio of implanted matrix atoms to the original number of precipitate atoms.

First, calculations were made to determine the trajectory of an average PKA after an elastic nuclear collision with a 14 MeV neutron. Next, precipitates of different sizes were placed at various points along the trajectory in order to maximize the probability of interaction between the cascade and the precipitate. Results of these calculations are shown in fig. 4, where the dissolution efficiency, η_{Dis}, is shown as a function of the radial position measured between the precipitate center and the initial PKA position. It is important to note here that for single cascade interaction with precipitates, the PKA initial direction is purposely chosen toward the precipitate, which is situated along its trajectory. The calculations show that average 14 MeV neutron collision cascades will completely destroy only small size precipitates, of the order of 10 Å diameter. Larger size precipitates may be partially destroyed, with an efficiency less than 100%, as shown in fig. 4. Fig. 4 shows a comparison between single PKA results and the results of a 100 history simulation for a precipitate diameter, $d = 30$ Å. The maximum dissolution efficiency is only ~ 7%, when cascades are started at approximately 100 Å away from the precipitate center. If the PKA is close to the surface of the precipitate, its displacement efficiency is low because the PKA and most of the recoils interacting with the precipitate are highly energetic. Therefore, the cascade constituents passing through the precipitate lose their energy to electrons rather than displacing or sputtering precipitate atoms.

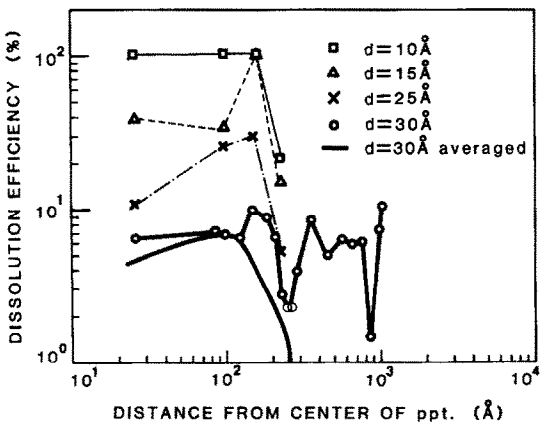

Fig. 4. Dissolution efficiency of $M_{23}C_6$ precipitates in steel as function of cascade initial position for various precipitate sizes.

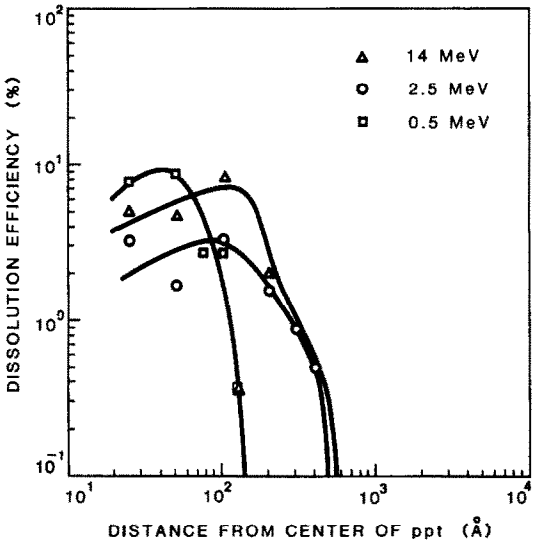

Fig. 5. Dissolution efficiency as function of distance between PKA and precipitate for PKA from different neutron energies, for 30 Å diameter precipitates.

Even though single cascade results show an increase in the dissolution probability toward the end of the PKA range, simulations of a sequence of cascades initiated randomly toward the center of the precipitate do not lead to this conclusion. Cascades initiated at distances larger than 200 Å from the precipitate center tend to "wander away" rather than hit the precipitate

The dissolution efficiency is shown in fig. 5 as a function of distance from precipitate center for a 30 Å diameter precipitate in 3 different neutron spectra, of average energies 0.5 MeV, 2.5 MeV and 14 MeV. Average PKA energies used in the calculations are shown in table 2. The efficiency is maximum for low energy neutrons (0.5 MeV), and whose initial collisions are within ~ 40 Å from precipitate center. Fig. 6 shows the implantation efficiency as a function of distance from the center of a 30 Å precipitate, again representing three

Table 2
Average PKA energies used throughout the calculations

Neutron energy	Material		
	Carbon	Iron	Molybdenum
0.5 MeV	71.0 keV	17.2 keV	10.2 keV
2.5 MeV	355 keV	86.4 keV	51.0 keV
14.0 MeV	1.99 MeV	484 keV	286 keV

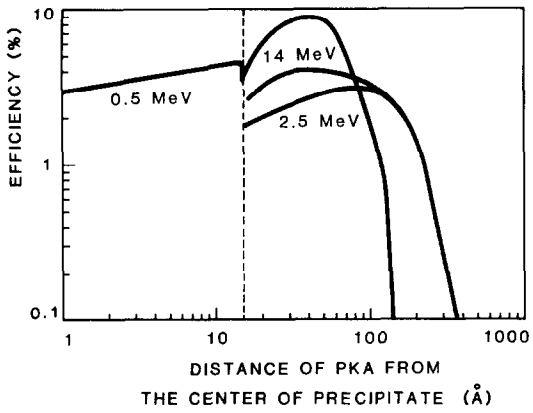

Fig. 6. Implantation efficiency as function of distance between PKA and precipitate for PKA from different neutron energies, for 30 Å diameter precipitates.

different neutron spectra. It is interesting to note that the implantation efficiency decreases as the cascades are initiated closer to the center of the precipitate.

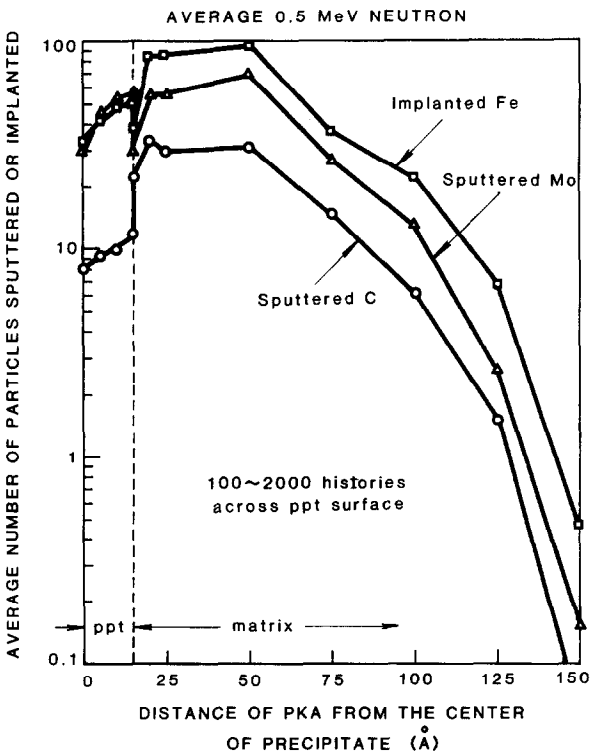

Fig. 7. Average numbers of sputtered (dissoluted) atoms, C and Mo, and implanted atoms, Fe, as functions of distance between PKA and precipitate for PKA from 0.5 MeV neutron, for a 30 Å diameter precipitate.

The energy transferred in a collision between two atoms depends primarily on the kinematic factor $\Lambda = 4M_1M_2/(M_1 + M_2)^2$. Maximum energy transfer can therefore occur between similar atoms. Fig. 7 is a plot of the average number of atoms sputtered away from the precipitate or implanted into the precipitate for average 0.5 MeV neutron cascades. It is shown that the number of implanted Fe atoms is greater than the combined number of sputtered Mo and C atoms in an $M_{23}C_6$ precipitate. Large mass differences between C and both Mo and Fe leads to less C sputtered into the matrix. It is expected, therefore, that cascades will lead to a slower depletion of C over Mo inside the precipitate. This is an important result since the stoichiometric composition of precipitates dictates their thermodynamic behavior.

5. Summary and conclusions

The present work is an extensive study of the problem of cascade interaction with precipitates. The study is based on the application of a newly developed Monte Carlo computer program, TRIPOS, for ion–solid interactions in multispecies media. Among the important features of this computer code are: (1) the use of continuous power law potentials; (2) inclusion of small angle nuclear collisions; and (3) the distance between collisions is variable and determined from a probability distribution. The main conclusions of the work are:

(1) Good agreement is obtained between the results of TRIPOS and surface sputtering experiments, as well as the codes TRIM and MARLOWE for sputtering, particle and energy reflection, and ion penetration.

(2) Neutron-initiated high energy collision cascades will completely destroy a precipitate whose size is only a small fraction of the cascade size. While the total path length of typical 14 MeV cascades is roughly 1500 Å in Fe, the maximum precipitate size that may be completely destroyed is on the order of 10 Å.

(3) There is a position, measured from precipitate center, where the dissolution and implantation efficiencies are maximum. Farther than this position, cascades "wander away" from precipitates, while cascades initiated inside or close to precipitates tend to penetrate the precipitate without causing much dissolution.

(4) Dissolution efficiency does not scale up with neutron energy. Maximum efficiency is for neutrons with energies on the order of 0.5 MeV.

(5) Differences in mass between precipitate atoms and matrix atoms lead to preferential cascade effects. The composition of precipitate elements lighter than matrix elements is not depleted as fast as heavier elements.

References

[1] A.C. Damask, in: AIME Symp. on Radiation Effects (Ashevill, North Carolina, 1965) p. 77.

[2] S.F. Pugh, in: the Interaction of Radiation with Solids, Summer School at Mol (North-Holland, Amsterdam, 1963) p. 261.

[3] R.S. Nelson, J.A. Hudson and D.J. Mazey, J. Nucl. Mater. 44 (1972) 318.

[4] J.A. Hudson, J. Br. Nucl. Energy Soc. 14 (1975) 127.

[5] P. Wilkes, University of Wisconsin Report, UWFDM-271 (1978); P. Wilkes, J. Nucl. Mater. 83 (1979) 66.

[6] K.Y. Liou and P. Wilkes, J. Nucl. Mater. 87 (1979) 317.

[7] G.R. Piercy, J. Phys. Chem. Solids 23 (1962) 463.

[8] K.B. Winterbon, Nucl. Sci. Eng. 53 (1974) 261.

[9] C.A. Coulter and P.M. Parkin, J. Nucl. Mater. 88 (1980) 249.

[10] O. Oen and M.T. Robinson, J. Appl. Phys. 35 (1964) 2515.

[11] T. Ishitani, R. Shimizu and K. Murata, Jap. J. Appl. Phys. 11 (1972) 125.

[12] J.E. Robinson and S. Agamy, in: Atomic Collisions in Solids (Plenum Press, New York, 1974) p. 215.

[13] J.P. Biersack and L.G. Haggmark, Nucl. Instr. and Meth. 174 (1980) 257.

[14] H. Attaya, PhD Dissertation, University of Wisconsin Report, UWFDM-420 (1981).

[15] G. Moliere, Z Naturf. A2 (1947) 133.

[16] K.B. Winterbon, P. Sigmund and J.B. Sanders, Kgl. Damske Videns. Selsk., Mat. Fys. Medd. 37 (1970) 14.

[17] P. Sigmund, Phys. Rev. 184 (1969) 383.

[18] O. Oen and M.T. Robinson, Nucl. Instr. and Meth. 132 (1976) 647.

[19] H.L. Bay and J. Bohdansky, J. Appl. Phys. 19 (1979) 421.